12-2019

Spark Plasma Sintering of Low Modulus Titanium-niobium-tantalum-zirconium (TNTZ) Alloy for Biomedical Applications

Nicholas Mavros

Taban Larimian

Javier Esqivel

Rajeev Kumar Gupta

Rodrigo Contieri

See next page for additional authors

Authors

Nicholas Mavros, Taban Larimian, Javier Esqivel, Rajeev Kumar Gupta, Rodrigo Contieri, and Tushar Borkar

Spark plasma sintering of low modulus titanium-niobium-tantalum-zirconium (TNTZ) alloy for biomedical applications

Nicholas Mavros, Taban Larimian, Javier Esqivel, Rajeev Kumar Gupta, Rodrigo Contieri, Tushar Borkar

HIGHLIGHTS

- Low modulus beta titanium alloys have been fabricated via ball milling followed by SPS using elemental blend powders.
- Bond order $\overline{BO}$ and energy level $\overline{MD}$ approach have been used to design targeted alloy compositions.
- All TNZT alloys exhibit large volume fraction of β-phase, which promotes attaining low elastic modulus.
- All TNZT alloys have shown promising corrosion resistant properties, which suitable for potential biomedical applications.

GRAPHICAL ABSTRACT

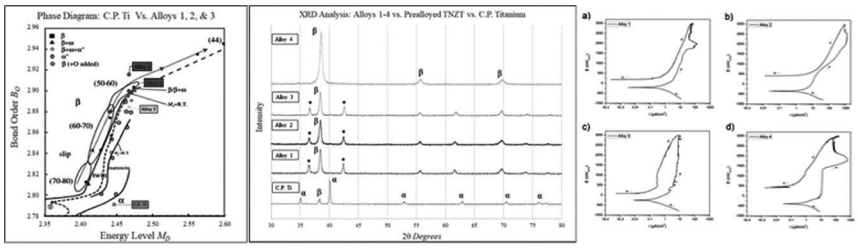

ARTICLE INFO

Article history:
Received 13 June 2019
Received in revised form
22 August 2019
Accepted 26 August 2019
Available online 27 August 2019

Keywords:
Low modulus beta titanium alloys
Mechanical alloying
Spark plasma sintering
Corrosion
Biomedical applications

1. Introduction

Over the decades since the industrial revolution, manufacturing and materials research and development have introduced new methods into the way scientists and engineers design solutions and

improvements to many technical challenges. In the field of biomechanics, specifically prosthetics and orthopedics, professionals are often tasked with adopting these advances in material science as solutions to thousands, if not millions, of patients. While progress has been made in numerous genres of engineering in the industry, all breakthroughs are made with the goal to improve patients' overall health and well-being. Presently, post-treatment rehabilitation continues to substantially influence the well-being of the patient, as this plays a role in the length of time that must be taken for the patient to return back to their normal routine. Recent developments in fields such as advanced manufacturing close the gap between time, cost, and more effective, unique solutions. The study of orthopedics and orthopedic surgery is a field that consistently operates at the forefront of available and proven technology. Advances in manufacturing, methods, and materials often pave the way for new medical applications that allow patients the opportunity for a healthier well-being. Orthopedic surgery that utilizes biocompatible materials to affix musculoskeletal supports or foundations is a practice that directly benefits from advances in material science and the methods which manufacture them. The Journal of Bone and Joint Surgery published a 2015 study from the Department of Health Sciences Research and the Department of Orthopedic Surgery at the Mayo Clinic of Rochester, Minnesota that investigated total hip and knee replacement surgeries in the United States. The study showed that in 2010, approximately 7.2 million total joint replacement surgeries were performed in the United States alone; 2.5 million being total hip replacements and 4.7 million total knee replacements [1]. This study is one of several that have observed arise of hip and knee replacements [1,2]. This data does not include the amount of other orthopedic surgeries regarding joint, hardware or dental implants or replacements, which suggests the demand for improved alloys exceeds those in total hip and knee replacements.

A large majority of the literature today regarding materials of construction for orthopedic implants focuses on well-documented alloys such as Ti-6Al-4 V. However, there are still challenges that need to be overcome that include issues of the mechanical strength and toxicity to neighboring tissues. While surgical or procedural negligence can increase the risk of incorrect fixation of joint replacements, pain or discomfort can be felt due to bone atrophy after some time, even if the procedure was a success. Studies have attempted to determine the reason for this, and have identified a phenomenon called “stress shielding.” The stress shielding phenomenon occurs when forces transfer between materials with a significant difference of elastic strength [3]. In other words, the bone will begin to atrophy or degrade, if they are not supplied with stress equivalent to everyday use. This is something astronauts have to work hard to avoid in microgravity. For excessively strong materials, bone atrophy occurs and leads to the loosening of the implant and refracturing of the bone [4]. This produces a feeling of discomfort over long periods of time and is explained by the difference in material performance between the implant and surrounding tissues [5]. Multiple sources suggest a solution to mitigate stress shielding is designing new alloys with a lower modulus of elasticity and improve ductility [6]. Currently, Commercially Pure Titanium (C.P. Ti) and $\alpha + \beta$ Ti-6Al-4V ELI (Extra Low Interstitial) alloys are widely used as a load bearing biomechanical implants due to the combination of specific strength, corrosion resistance, and their relatively high biocompatibility. However, their application for long term use is limited due to issues like stress-shielding, leaching of Al and V ions which may cause health issues like peripheral neuropathy, osteomalacia, and Alzheimer's disease [3,7–9]. Thus, there is an imminent need to develop newer implants with superior properties. The ideal candidate alloy for a hip implant procedure should exhibit excellent biocompatibility with no adverse tissue reactions, excellent corrosion resistance in the body fluid, high strength and fatigue resistance, low modulus, low density, and exceptional wear resistance. Unfortunately, very few alloying elements are biocompatible when implanted in the human body. These include Titanium, Molybdenum, Niobium, Tantalum, Zirconium, Iron, and Tin [4]. Other elements such as Gold, Platinum, and Palladium also offer good biocompatible properties, though the cost of these metals begins to affect their practicality. It also has been reported that the addition of Zr, Nb, Mo, Hf or Ta elements increase the strength and decrease the modulus of body-centered cubic (BCC) β-phase Ti alloys [5,10]. Thus, a new β-phase titanium alloy based on the Ti-Nb-Zr-Ta, or TNZT, system has been developed with an aim to achieve low rigidity, effective bone healing, and remodeling. Another incentive for further research in alternative materials is the biocompatibility of the elements present in the alloy. Recent studies show that the release of both Vanadium and Aluminum ions from Ti-6Al-4V might cause long-term health problems such as peripheral neuropathy, osteomalacia, and Alzheimer diseases [10,11]. Selecting elements to optimize biocompatibility have been shown to yield beneficial properties regarding tissue growth around implants. One study, in particular, focused an observation on bone tissue regeneration in tibial fracture sites on rabbits, where intramedullary rods of various common biomedical materials were introduced, including a TNTZ alloy [12,14]. Here, the study mentioned the fracture callus for a Ti-29Nb-13Ta-4.6Zr specimen contained little to no signs of fracture after just 10 weeks of healing, which was slightly quicker than the Ti-6Al-4V specimen, and much quicker than the 316 L specimen which continued to show healing evidence after 22 weeks.

Mechanical alloying (MA) that has been established over the past three decades has received special attention as a viable and powerful alternate processing route for the synthesis of amorphous and nanocrystalline materials [15–27]. Mechanical alloying (MA) is a powder processing technique that allows the production of homogeneous materials from the elemental blend powders. MA is a solid-state powder processing technique involving repeated welding, fracturing, and rewelding of powder particles in a high-energy ball mill. Powder metallurgy is a novel route for producing nanocrystalline alloyed powders suitable for compaction and consolidation. Mechanical alloying (MA) has gained special attention as a powerful non-equilibrium process for fabricating amorphous and nanocrystalline materials, whereas Spark Plasma Sintering (SPS) is a unique technique for processing dense and near net shape bulk alloys with homogenous microstructure [28–34]. Spark plasma sintering is a novel tool for processing of metals, alloys, and composites at lower temperatures and shorter processing times, as compared to conventional processing routes. Though SPS is particularly suitable within research and development domains, advanced materials continue to drive product optimization in nearly all fields, which has paved an avenue for SPS out of the research genre and into mass production environments. Biomedical metals are typically made from cast or wrought processes, while many research institutions may use Vacuum Arc Melting (VAM), Hot Isostatic Pressing (HIP), or SPS. Of these, SPS is increasing in popularity as an advanced manufacturing technique. While the concepts utilized in SPS technology have been used for decades, it continues to stimulate interest in the material science field and has had a steady increase in research articles since the turn of the millennium [9]. Compared with traditional manufacturing methods, the efficiency of the SPS process is what summarizes the main benefits of the process and why this method is preferred among many research institutions. Its ability to create exotic materials that are difficult to synthesize using conventional methods is particularly useful in material development.

The main objective of this work is to study the effect of different alloying elements on microstructure, phase transformation and mechanical properties of these newly developed β-phase titanium

alloys and establish new avenues for the future development of biocompatible titanium alloys with optimum microstructure and properties.

2. Material selection

Titanium is a versatile elemental metal and can be alloyed with many different elements to produce alloys that are ideal for a multitude of industries. The medical and aerospace industries, in particular, are those which take advantage of the high strength and low weight of these types of materials. Ceramic reinforced titanium composites can be used in high-temperature applications, particularly in jet and rocket engines. Regardless of their application, titanium alloys are classified based on their microstructural phases at atmospheric conditions. These categories are α, near-α, $\alpha+\beta$, metastable β, or stable β-phases [10]. These phases significantly affect the mechanical properties of titanium alloys. The use of titanium for implant materials of construction is not new, with the official patents filed in the 1960s [13]. The idea of using electric current to sinter metals was first conceived nearly a century ago [14]. Though research primarily took place with dentistry in mind, titanium itself possesses a unique relationship with bone tissue that many other materials lack. Titanium is able to fully osseo integrate within the bone, even around material surface irregularities. As defined, osseo integration is the direct anchorage of an implant by the formation of bony tissue around the implant without the growth of fibrous tissue at the bone-implant interface. Another advantage to titanium is the natural formation of a thin oxide layer, which has been shown to be beneficial as a foundation for natural tissue [35]. The alloying of titanium to produce a material suitable for in vivo purposes has been well studied in the past. As previously mentioned, long term studies are imperative to observe the biocompatibility of the alloy, as chemical reactions in the body in this regard can take place over a number of years. Nonetheless, other test methods are available to effectively evaluate candidate materials prior to long term tests such as clinical trials. Fig. 1 shows a study done by Kuroda et al., where a cell culture analysis was performed on pure elements [8]. Fig. 1(b) shows that there is a trend between the polarization resistance of these pure elements and their degree of biocompatibility. This evidence supported the decision to move forward with material design with

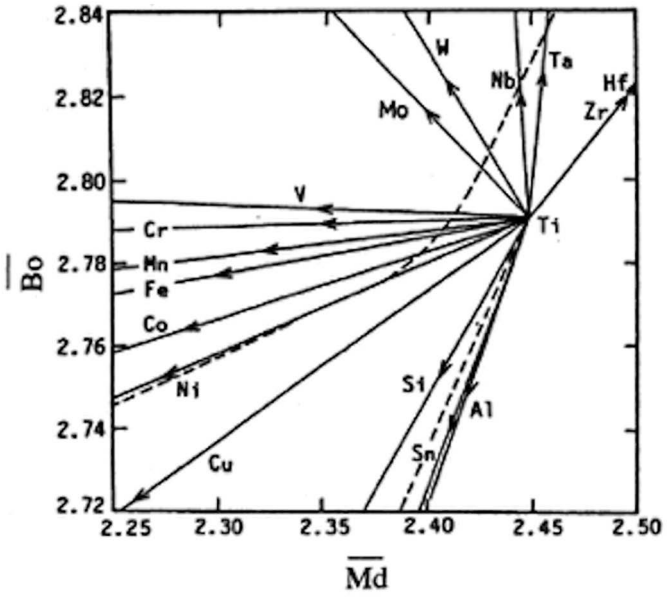

Fig. 2. Effect of alloying elements on CP Titanium.
(Reprinted with permission from Kuroda, D., Niinomi, M., Morinaga, M., Kato, Y., & Yashiro, T. (1998). Design and mechanical properties of new β type titanium alloys for implant materials. *Materials Science and Engineering: A*, *243*(1–2), 244–249.)

elements in the upper right quadrant of Fig. 1(a) and (b). It should be noted that the quantity of elements within the body is considered acceptable, as this also affects cytotoxicity. For example, Manganese has been used as an alloying element in some metallic alloys for biomedical applications. However, it has been found in one study reviewing applications of Ti–Mn alloys that those containing 18% mass of Manganese showed signs of cytotoxicity, while alloys with 14% mass were shown to be acceptable [36].

Moringa et al. [8,37,38] have developed a method for proposing new titanium alloys based on a molecular orbital approach using electrical properties of materials, more specifically, the bond order and d-orbital energy (Fig. 2). As other elements are added, the bond order and d-orbital energy changes, assuming complete chemical homogeneity are achieved. Bond order, identified by $\overline{B}_O$, is a

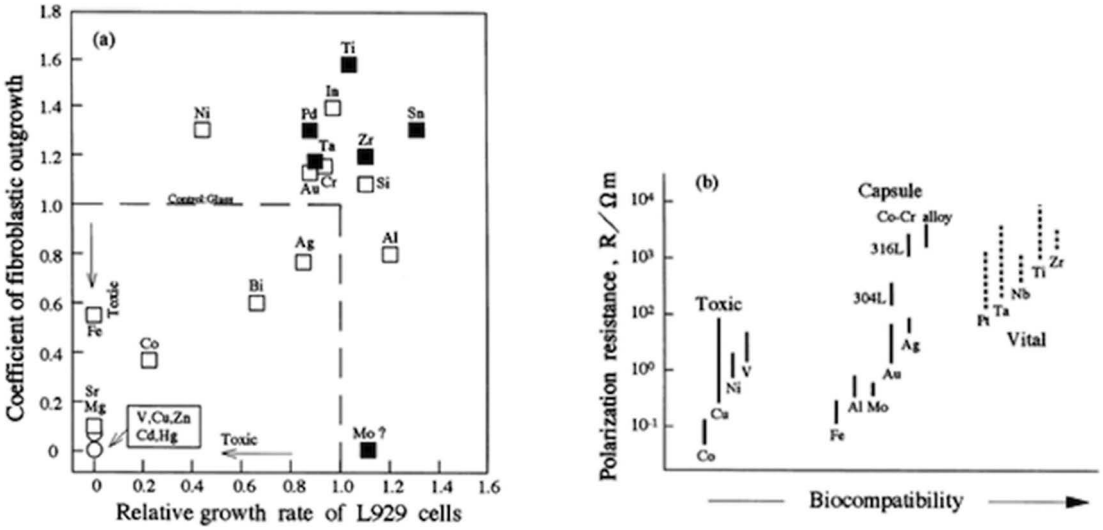

Fig. 1. Cell culture study of pure elements in (a) and the relationship between polarization resistance and biocompatibility of elements and metals in (b).
(Reprinted with permission from Kuroda, D., Niinomi, M., Morinaga, M., Kato, Y., & Yashiro, T. (1998). Design and mechanical properties of new β type titanium alloys for implant materials. *Materials Science and Engineering: A*, *243*(1–2), 244–249.)

Table 1
Alloy compositions and corresponding calculated $\overline{B}_o$ and $\overline{M}_D$ values.

Alloy ID	Elemental Composition %wt					
	Ti	Nb	Zr	Ta	$\overline{B}_o$	$\overline{M}_D$
Alloy1 (Ball milled)	45	30	5	20	2.899	2.467
Alloy 2 (Ball milled)	40	35	5	20	2.915	2.467
Alloy 3 (Ball milled)	53	35	7	5	2.884	2.467
Alloy 4 (Pre-alloyed)	53	35	7	5	2.884	2.467
C.P. Ti	100	0	0	0	2.790	2.447

measure of the strength of the covalent bond between titanium and other elements; each pure element has a measure of the strength between atoms. The energy level, identified by $\overline{M}_D$ is a correlation of the electronegativity and the metallic radius of elements. UNSR50250 or ASTM Grade1 titanium, otherwise known as C.P. Ti, is estimated to have a $\overline{B}_O$ of 2.790 and an $\overline{M}_D$ of 2.447 eV. This corresponds to a Young's Modulus of approximately 116 GPa [39]. There are multiple grades of C.P. Titanium, however, the mechanical properties are relatively similar between the grades. Alloys of titanium vary considerably in terms of their mechanical properties, even when only observing those suitable as a biocompatible material.

$$\overline{B}_O = \sum_{n=1}^{i} X_i B_{oi} \tag{1}$$

$$\overline{M}_D = \sum_{n=1}^{i} X_i M_{di} \tag{2}$$

The $\overline{B}_O$ and $\overline{M}_D$ represented in Eqs. (1) and (2) are simply weighted averages of the properties of the alloying elements, where X_i represents the atomic fraction of the i^{th} element in the alloy. As previously stated, titanium is an excellent material regarding its resistance to corrosion in vivo; the issue resides in the elastic modulus and particularly the differential between that and the elastic modulus of human bone. The corrosion of materials is inevitable. However, it is well understood that certain families of materials will resist corrosion more effectively than others. Typically, we associate corrosion with outdoor moisture resulting in the buildup of oxides, hydroxides, etc. This natural process is not excluded from in vivo implants, and since the material must retain its biocompatibility, it is not permitted to receive the same surface treatments and coatings that are suitable for metals exposed to more common applications. Though the environment in which implant material is installed contrasts these more common applications, the corrosion process is similar and has been extensively studied and well understood for in vivo procedures. Using the compositions provided in Table 1 we can estimate how this corresponds to the phase and approximate modulus of elasticity. Fig. 3 shown below provides an illustration of where the alloys are expected to land on the bond order and energy level diagram. A strong β-phase around the 50–60 GPa range was targeted.

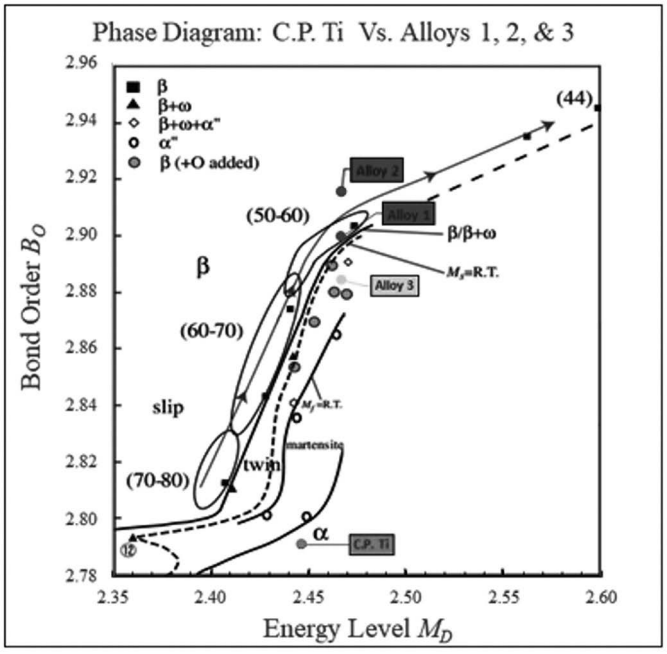

Fig. 3. Estimation of phase region for material candidates.
(Reprinted with permission from Kuroda, D., Niinomi, M., Morinaga, M., Kato, Y., & Yashiro, T. (1998). Design and mechanical properties of new β type titanium alloys for implant materials. *Materials Science and Engineering: A*, *243*(1–2), 244–249.)

3. Experimental details

The elemental powders of titanium (<8 mm, 99.5%), niobium (<8 mm, 99.5%), tantalum (<8 mm, 99.5%), and zirconium (<8 mm, 99.5%) were used as starting materials. The powders were mixed to the nominal compositions as shown in Table 1. Alloy 4 has same composition as alloy 3. However, alloy 4 has been obtained via SPS processed pre-alloyed TNZT powder, whereas alloy 3 has been obtained via SPS processed ball milled elemental blend powder. The mixture was weighed and loaded in a tungsten carbide vial with tungsten carbide balls to give a ball to powder (BPR) ratio of 10:1. The powders were mechanically alloyed for 60 h. under an argon atmosphere in a planetary ball mill (Fritsch Pulverisette 7) with a rotational speed of 300 rpm without the addition of any process control agent in order to avoid contamination of the powders. The milling process was interrupted each ½ h for ¼ h in order to avoid local temperature rising inside the vials as well as cold welding. The mechanically alloyed TNTZ powders were pre-compacted in a graphite mold under a pressure of 5 MPa. The pre-compacted powders were sintered by an SPS system at a temperature of 1373 K for 5 min under a controlled argon atmosphere under a pressure of 50 MPa. The heating rate was maintained at 100 °C/ min. These SPS sintered TNTZ alloys were characterized in a FEI-Quanta Nova-SEM. The phase compositions of milled powders and the sintered samples were characterized by X-ray diffraction (1.54 Cu Kα) line of a Rigaku Ultima III X-ray diffractometer. The microhardness of SPS processed samples were measured using a standard Vickers microhardness tester under a load of 1.96 N for 15 s. Average of 10 readings were taken into account. The dynamic elastic modulus (E) was obtained from the impulse excitation technique based on the ASTM-E1876 technical standard using ATCP Sonelastic® Equipment. The measurements were performed 5 times in each sample to ensure measurement accuracy. The corrosion behavior of the designed SPS processed alloys was studied by cyclic potentiodynamic polarization tests. The response to cyclic potentiodynamic polarization of SPS processed

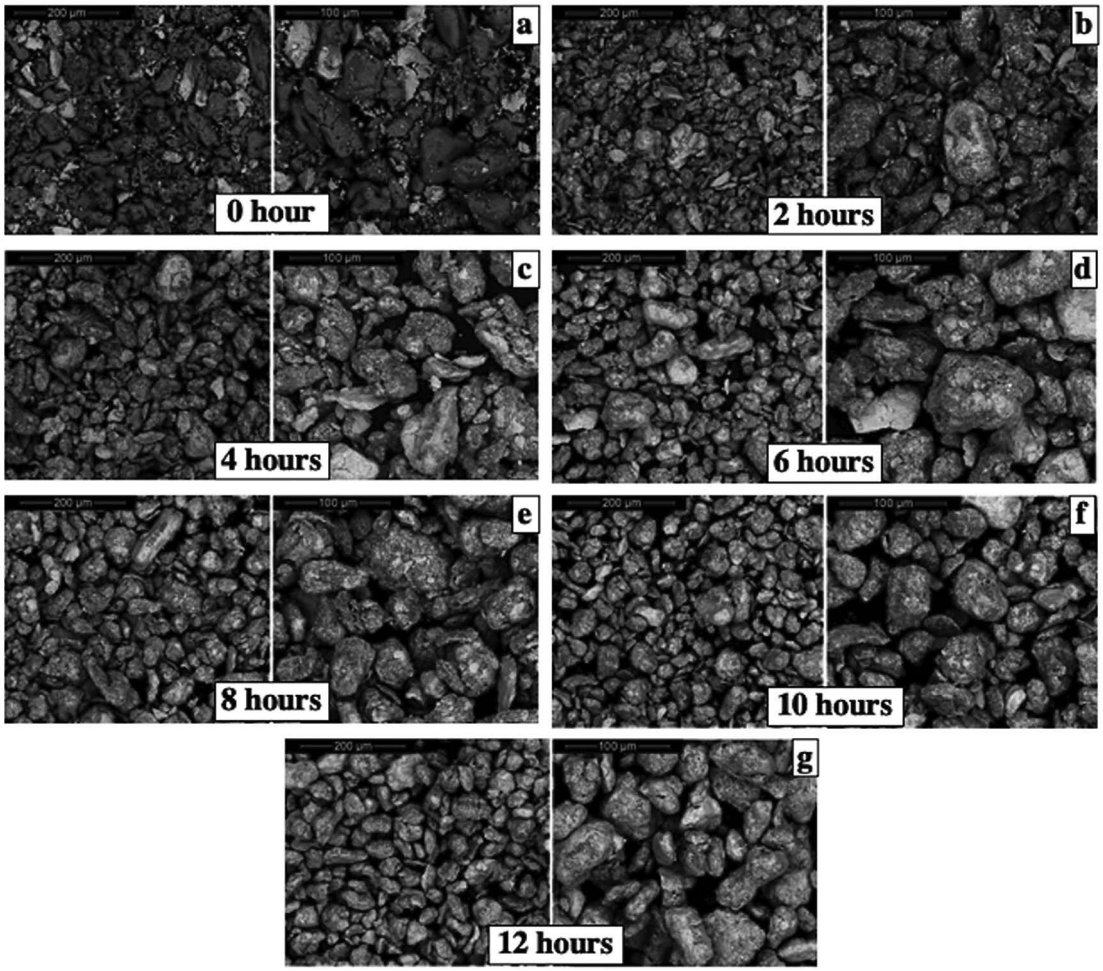

Fig. 4. SEM images of ball-milled powder of TNTZ alloy 1 for (a) 0, (b) 2, (c) 4, (d) 6, (e) 8, (f) 10, and, (g) 12 h.

samples was compared to the commercially pure titanium (C. P. Ti) that is widely used in orthopedic applications. A typical three-electrode cell configuration was used consisting of an SPS processed TNZT alloy, as a working electrode, Saturated Calomel Electrode (SCE) as a reference electrode, and platinum foil as the counter electrode. Each test run was performed in a fresh 0.5 M NaCl solution. The potential scan rate was 1.0 mV/s, starting from a fixed potential of -0.75 mV_{SCE}, and upwards until 3.00 V_{SCE}. Upon reaching the potential of 3.00 V_{SCE}, the scan was reversed downwards until cathodic current densities were encountered.

4. Results and discussion

4.1. Microstructure

Due to the lack of evidence or mathematical models to estimate exact ball milling parameters, a trial-and-error approach was taken to understand the effects of milling parameters (ball-powder weight ratio, rotational speed, time, quantity, ball size, process atmosphere, etc.) on the alloying of TNZT alloys. An experiment was performed to assist in identifying operational parameters for the ball milling process. The procedure was to remove a small amount of powder after varying milling times to be viewed with SEM imaging and conduct a particle size analysis. The main objective was to optimize and identify milling parameters for TNZT alloying. In addition, identifying when the aforementioned agglomerated particles begin to break down and homogenize in size and shape was also investigated. A TNZT alloy was chosen for the experiment; in this case, Ti-35Nb-7Zr-5Ta, a composition identical to Alloy 3. Other results from other experiments provided enough insight to specify process variables such as milling time, rotational speed, etc. Every 2 h, the milling process was paused, a small 2−3-gram sample was removed, and then the milling vessel was replaced in the mill and process was continued. This continued until the powder underwent 12 h of total milling time. Fig. 4 shows SEM images of mechanically alloyed powder taken at the 0, 2, 4, 6, 8, 10, and 12-hour stages within the ball milling cycle. Additionally, SEM imaging in one source shows that after 5 h of milling 50 μm powders for a TNZT alloy, particle size and shape became irregular and agglomerated, while increased milling time under the same conditions showed particle homogenization around 80 μm [5,9]. While the images show particle agglomeration and breakdown, synthesizing under SPS conditions revealed an inconsistent dispersion of elements. This could have been due to the ball milling parameters chosen. However, it was noticed that as the milling time increased further to 24, 48, 60, and 100 h, elemental homogenization was eventually achieved. Reviewing the SEM imaging in Fig. 5 shows adequate alloying. Alloy 1 appeared to retain the highest degree of homogeneity among the specimens using mechanical attrition. Observation of the results showed marginal differences between the microstructure of alloys 1, 2, and 3. This was determined by the grain geometry and sizes observed in Fig. 5, as they appear

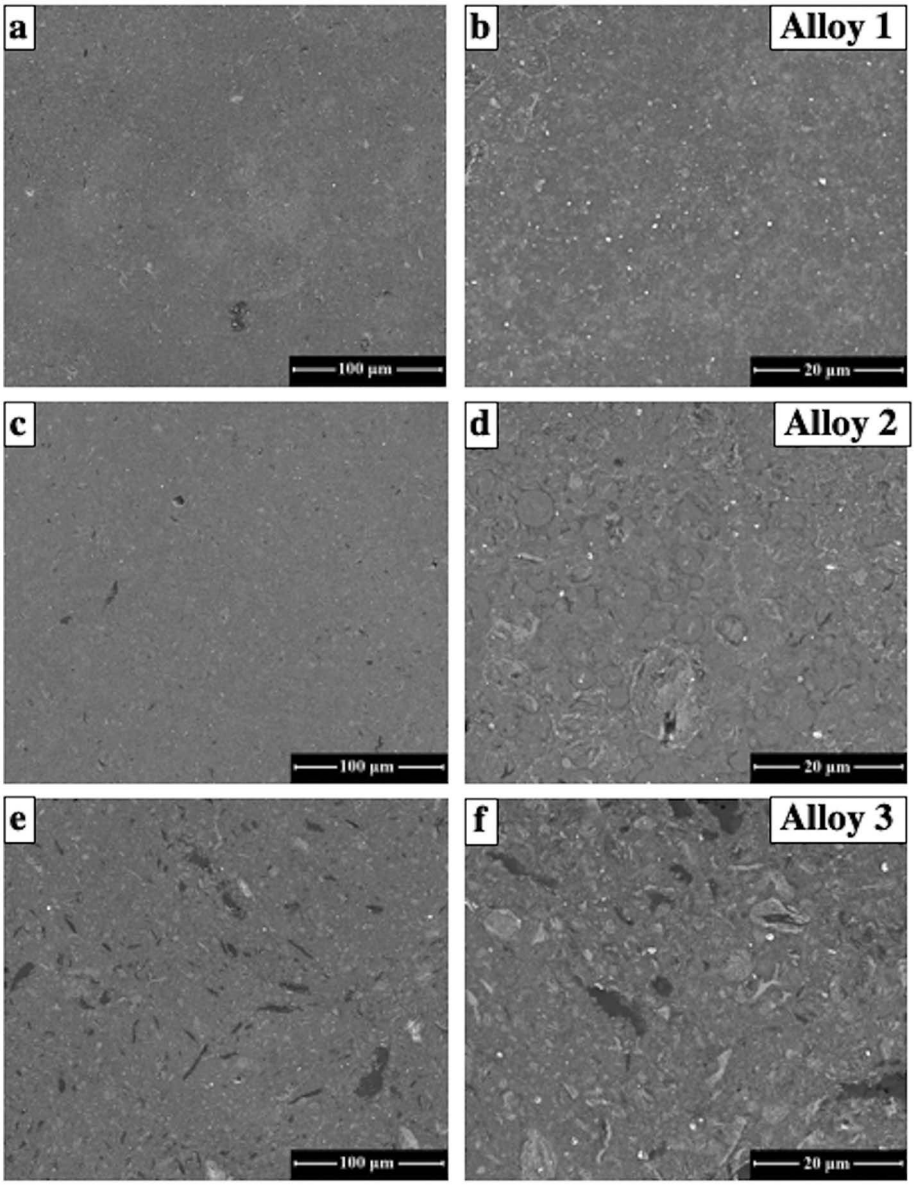

Fig. 5. SEM images of alloy 1 (a and b), 2 (c and d), and 3 (e and f).

anisotropic and erratic in shape. When comparing microstructures of these alloys with the referenced works, standard and backscatter images show clusters of grains of β-phase Ti, with intergranular α-participants which appear more pronounced [8,11,40]. A majority of the papers referenced utilized vacuum arc melting or HIP to manufacture specimens directly from raw material buttons or small ingots, which involve complete melting of the material, as opposed to sintering the particles together at a temperature considerably lower than the materials full melting temperature. Among all variables, the SPS processing method appeared to cause the biggest change in microstructure, as completely melting the ball milled particulates would most likely eradicate any remaining material characteristics imposed from the ball milling process. Fig. 6 shows SEM images of SPS processed alloy 4 and C.P. Ti. Alloy 4 exhibited coarse grain microstructure corresponds to single phase BCC. However, when we have observed dark spot form Fig. 6(a) at higher magnification, fine-scale α-laths have been observed in Fig. 6(b). Fig. 4(c and d) shows SEM images of SPS processed commercially pure titanium. C.P. Ti exhibited a large volume fraction of BCC β-phase along with some fine-scale α-laths.

4.2. X-ray diffraction analysis

Diffraction patterns of mechanically alloyed as well as SPS processed TNZT alloys are shown in Figs. 7 and 8. Fig. 7 shows XRD patterns of SPS processed alloy 1 from mechanically alloyed powders for 24, 48, and 60 h. The X-ray diffractions patterns clearly show large volume fraction of BCC β-phase along with some minor HCP α-peaks. As milling time increases, the XRD pattern of an alloy 1 shows the presence of additional peaks corresponds to HCP α-phase or intermetallic phases. All the peaks are consistently indexed based on BCC β-phase. This was expected since all the alloys exhibit higher concentrations of β-phase stabilizing elements. On the other hand, XRD patterns of C.P. Titanium shows the presence of HCP α-phase regions. The results shown in Fig. 8 identify the β-phase as being the predominant phase in Alloys 1, 2, 3, and 4. C.P. Titanium is shown to be comprised primarily of the α-phase configuration. Alloy 4 which was SPS processed from pre-alloyed

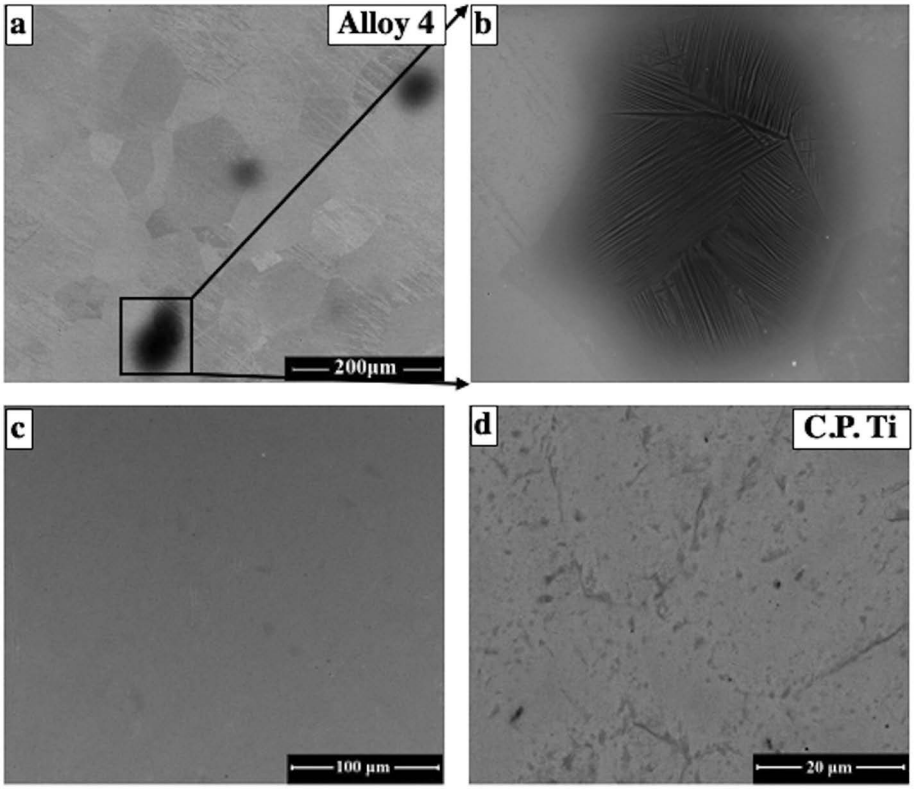

Fig. 6. SEM images of alloy 4 (a and b) and CP Ti (c and d).

powders shown only BCC β-phase as compared to alloy 1–3 which have been SPS processed from mechanically alloyed elemental blend powders. Observation into Fig. 8 shows small peaks, identified by the asterisks, surrounding the primary β-phase peaks appear to contain measurements that do not correspond with β-phase crystallography. Research by Hussein et al. on the Ti-Nb-Ta based systems detected α-phase precipitations around the primary β-phase matrix [41]. The peaks found in the study by Hussein et al., measured on a Ti-30Nb-18Ta alloy, have similar 2θ measurements as the peaks identified in Fig. 8. Considering the TNZT alloys in this research is relatively close in wt% of the referenced literature, this may suggest the peaks contain similar α'' phase

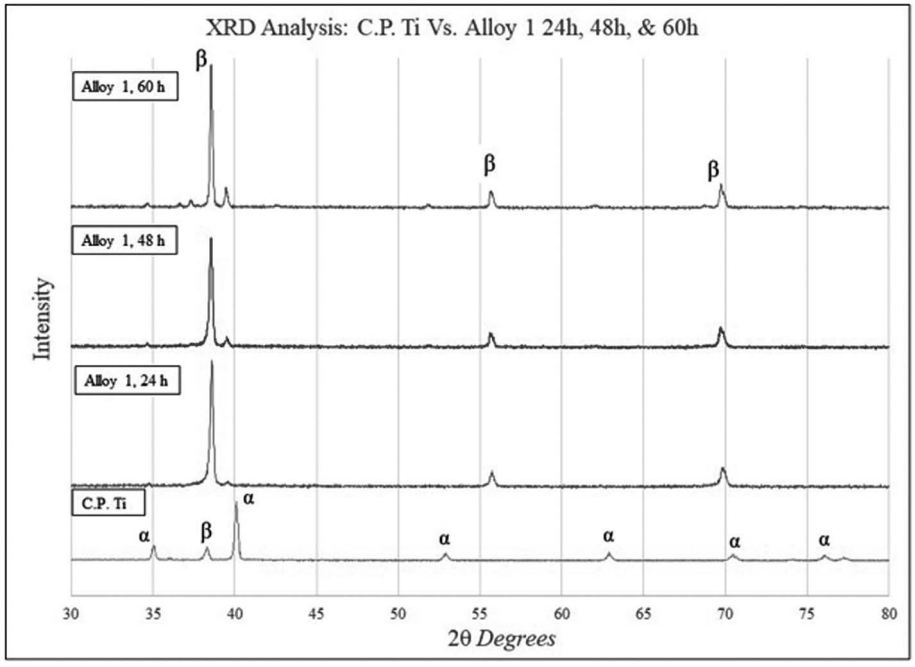

Fig. 7. XRD of ball-milled powder with varying timings.

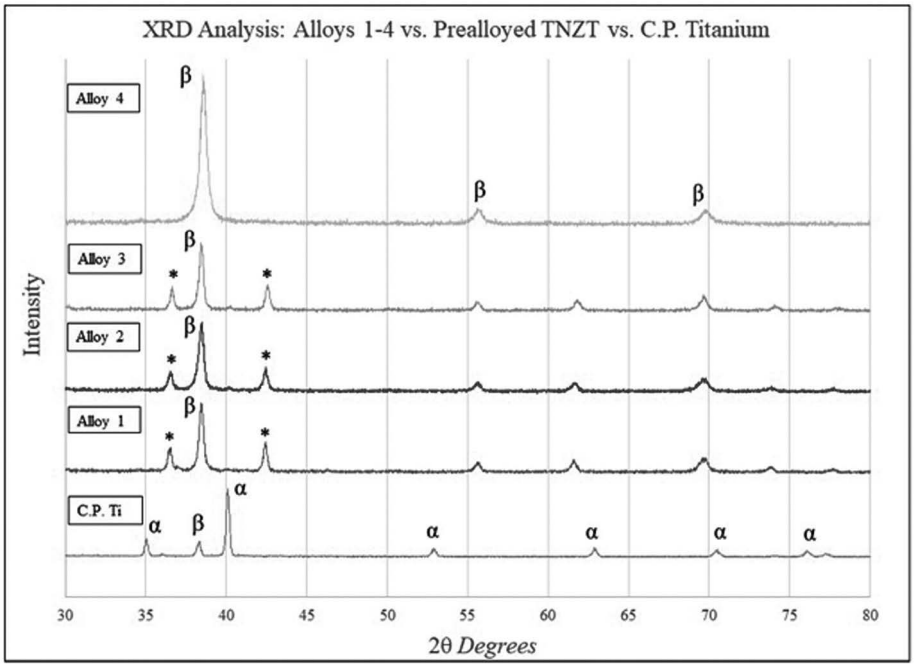

Fig. 8. XRD of alloys 1, 2, 3, and 4.

precipitations. However, additional XRD investigation is necessary to conclude and confirm this observation. All samples were manufactured under identical conditions, however, the raw material for Alloy 4 consisted of pre-alloyed TNZT particles. The difference in processes leading up to SPS synthesis could contribute to the differences in the XRD profiles.

4.3. Microhardness and modulus of elasticity

Vickers microhardness values of SPS processed TNZT alloys are listed in Table 2. All mechanically alloyed SPS processed alloys 1–3 exhibited higher microhardness as compared to alloy 4 processed via pre-alloyed TNZT powders as well as C.P. Titanium. Even though Alloys 1–3 exhibited large volume faction of BCC β-phase, crystallite sizes of these alloys are in the nanometer range due to mechanical alloying, which leads to very high microhardness as compared to alloy 4 and C.P. Titanium. Banerjee et al. reported hardness and modulus values of Ti-35Nb-10Zr-5Ta with and without precipitation hardened (aging), manufactured with a vacuum arc melter. Here, hardness and modulus values were 291 HV and 100 GPa without aging, and 258 HV and 89 GPa after an aging process, respectively [40]. The same alloy in this research (Alloy 3), manufactured under SPS conditions with mechanically alloyed powder yielded hardness values nearly twice as much as the results in the mentioned paper. However, hardness values for the same alloy with pre-alloyed powder (average 181 HV) yielded values slightly lower than reported by Banerjee. This suggests the difference in preprocessing, i.e. mechanical attrition as opposed to melting button-sized pieces of individual elements to homogenize the materials, will vary the hardness of the material. A TNZT powder identical in composition to Alloy 3 and 4 mechanically alloyed and processed using a similar SPS process was found to yield micro-hardness values between 650 and 660 HV [9]. The results identified in Table 2 show an average microhardness reading of 634 HV with mechanically alloyed TNZT powder. Grain boundaries present in the microstructure of materials are known sites of dislocation during the application of stress. While the decrease of grain size increases the number of dislocation sites, this also increases the surface area between grains, which also increases the hardness of materials, especially for anisotropic grain structures. Valiev et al reported a substantial increase in hardness and elastic modulus of Grade2 C.P. Titanium when comparing course grained versus ultra-fine-grained microstructures of the same metal [42]. The SEM images shown in Fig. 5 confirm very refine microstructure with nano grain sizes which may impede dislocation and generate the high hardness values seen in this work. While the strong β-phase stabilizers, Nb and Ta, are present in the alloys, α-phase participates still exist within the samples, which was presumed to increase hardness and elastic modulus. Hussein et al. reported that O has been known to promote higher hardness readings when added to solutions of Ti-Nb-Ta based [41]. The hardness results for the alloys produced using the ball milling method showed values considerably higher than the specimen manufactured with pre-alloyed powder, Alloy 4. These alloys are identical in composition to Alloy 3. Considering these materials were manufactured under identical conditions, this suggests that the ball milling process influenced the hardness of the alloys. This could be due to the fact that the mechanical attrition process essentially cold-works or work hardens the material together, a process frequently used in the industry to increase the hardness of a material. Considering the extent of the change in agglomerate diameters within the first 12 h of mechanical attrition, it can be inferred that the bulk of the cold-working hypothesis may take place within this time frame. This also corresponds to work done by Suryanarayana, stating that increasing milling time will work harden the particles, where the hardness and brittleness will increase [20].

Table 2
Vickers microhardness and Elastic modulus of SPS processed alloys.

Alloy ID	Vickers 0.1 kg microhardness, HV	Elastic modulus (E), GPa
Alloy 1	608±5	126±3
Alloy 2	571±4	149±2
Alloy 3	547±6	60±1
Alloy 4	173±4	66±1
C.P. Ti	246±5	115±3

On the elastic modulus results, Table 2 shows the values obtained. Note that for the Ti-CP the modulus of elasticity was in agreement with the literature, 115 ± 3 GPa [43]. As for alloys 3 and

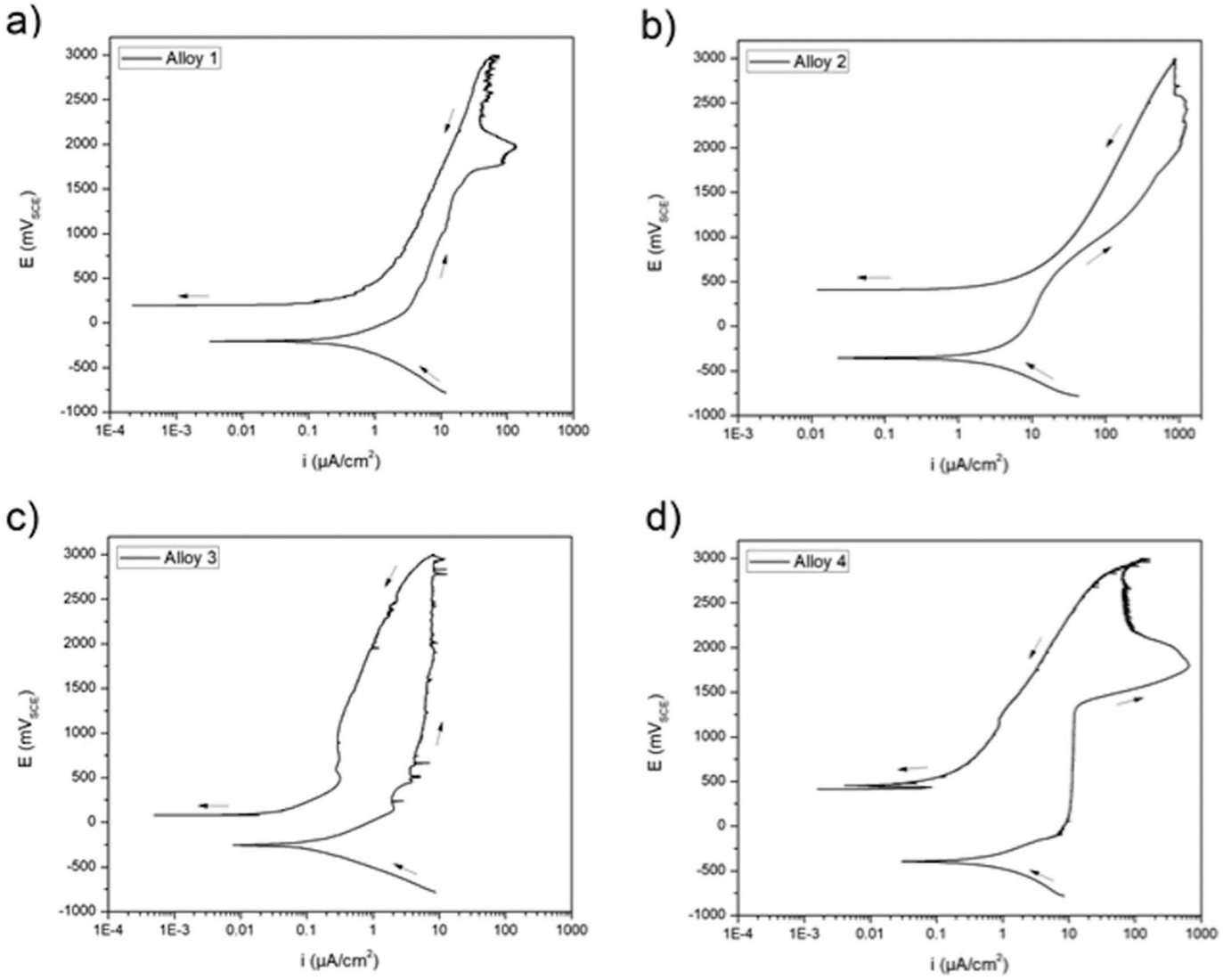

Fig. 9. Potentiodynamic polarization of SPS processed alloys and C.P. Ti, a) forward scan and b) backward scan.

4, despite the differences found in the X-ray diffraction pattern, we can say that the values were practically equal within the error range, being 60 GPa and 66 GPa respectively for alloys 3 and 4. Therefore, it is stated that, regardless of the processing route used, i.e. from the pre-alloy or the mixture of powders, the final result was the same, being, therefore, the SPS technique effective for the range of composition and process parameters used. However, for larger Ta fractions, modulus of elasticity values were relatively higher at alloy 1 (126 GPa) and alloy 2 (149 GPa). By analyzing the results of electron microscopy and X-ray diffraction, it can be assumed that the higher values of elastic modulus are related to the existence of a greater fraction of the alpha phase. According to studies reported by Souza et al. [44] depending on the cooling rate imposed on the Ti-Nb-Ta alloys, the modulus values are changed, being higher for slower cooling rates and lower for faster rates, for example, furnace and water cooling respectively. Samples processed by SPS have lower cooling rates, which according to studies reported by Zhang et al. [45], rates can reach 6.9 °C/s (high compared to furnace cooling of ~0.002 °C/s). Unlike rapidly cooled samples in water (~100 °C/s). Thus, comparatively, it can be stated that higher rates tend to stabilize more strongly, phases out of equilibrium conditions, being basically titanium beta phase, or alpha DP (equiaxed β grains with approximately 150 HV, or alpha needles within beta grains). On the other hand, decreasing the rate, the transformation approaches the equilibrium, i.e. alpha phase at room temperature (alpha needles grains with approximately 250 HV). As the SPS process entails intermediate cooling rates, between furnace and water cooling, the result found is consistent. In addition, it should be emphasized that, due to the fact that the cooling rates are lower than that of a water quench, the values obtained for modulus of elasticity are different from those found in the Bo vs. Md, which is proposed for rapidly cooled samples.

4.4. Corrosion behavior

Cyclic potentiodynamic polarization curves in 0.5 M NaCl solution for the designed SPS processed alloys, as well as CP Ti, are shown in Fig. 9. C.P. Ti and Alloy 3 exhibited a small increase in current densities with increasing potential applied. This behavior is typical of pure Ti and is indicative of good corrosion resistance. The feature described as the breakdown potential is clearly seen in the anodic scans for Alloys 1 and 4. The corrosion current densities, as calculated using Tafel extrapolation of cathodic curve, for the Alloys 1, 3 and 4 were similar (varied in between 0.4 and 0.7 μA/cm^2) whereas the alloy 2 exhibited higher corrosion density (2 μA/cm^2). Comparing the anodic curves, Alloy 2 shows the highest anodic

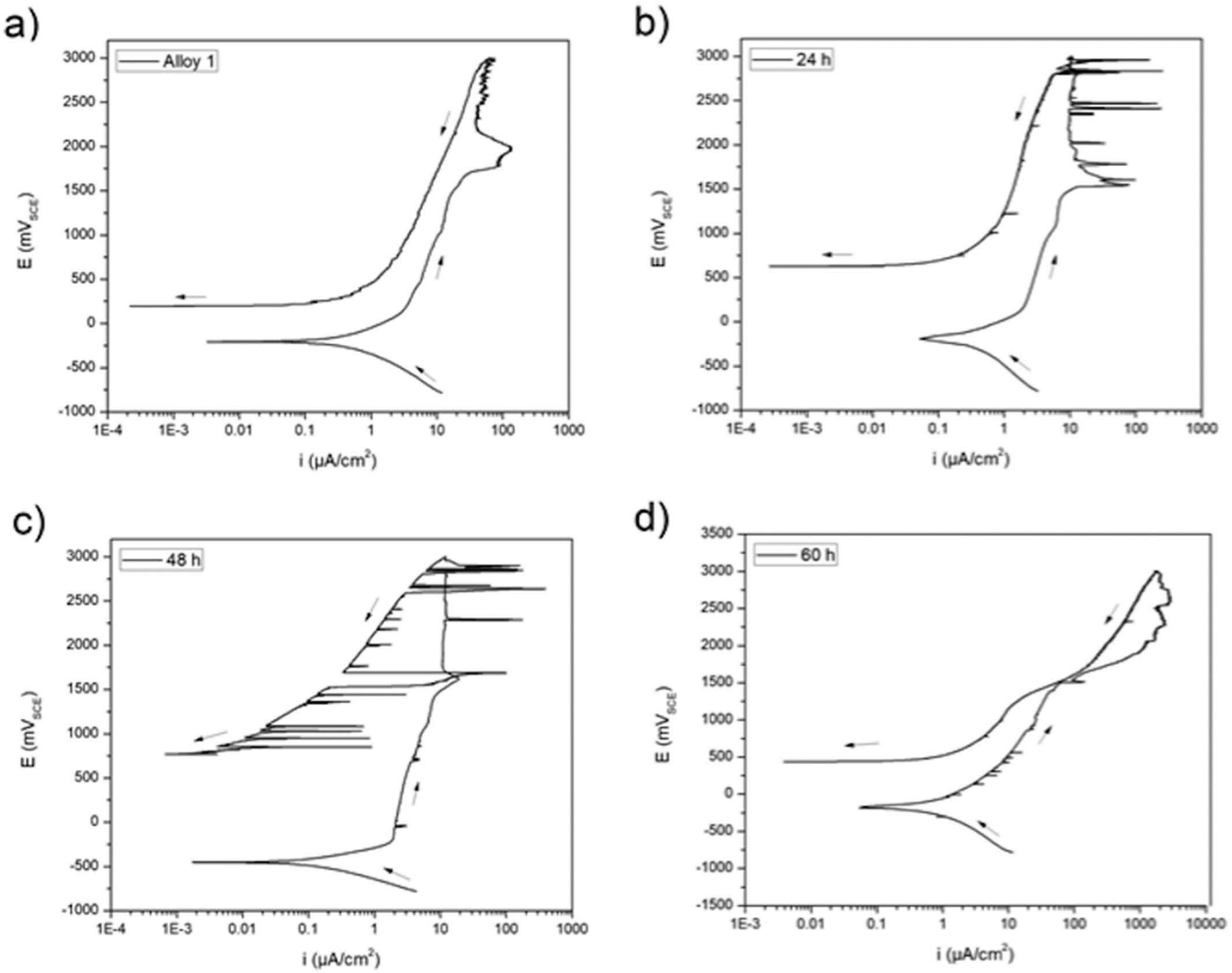

Fig. 10. Potentiodynamic polarization of SPS processed alloys and C.P. Ti, a) forward scan and b) backward scan.

current density followed by Alloy 4, Alloy 1, C.P. Titanium, and Alloy 3. Alloys readily decrease in anodic current density with decreasing applied potential during the reverse scan. The current densities in the reverse scan are smaller than those of the forward scan at the same potential, indicating a strong repassivation tendency. This behavior was observed even in alloys 1 and 4, which exhibited a breakdown potential, suggesting a strong repassivation tendency. A study done by Long and Rack mentions Nb and Zr contribute to the formation of a highly protective passive film on Ti alloys and are not released into the environment as dissolved metal ions. However, they go on to explain that surface oxide composition and/or distribution will affect the corrosion response of orthopedic alloys, and that characterizations of these oxide layers are required to understand and optimize the biocompatibility of Ti alloys [6]. Ti naturally forms an oxide layer, TiO_2, which is present in alloys of Ti, including the TNZT alloys in this research. Additionally, Nb and Zr present in TNZT alloys facilitate the development of highly protective passive layers, which lowers potential in an electrochemical interaction [46]. It was noted in another study that TNZT alloys will consist of $Nb_2O_5$and Ta_2O_5films, which are very stable, and inhibit electron exchanges between the material and environment [41]. Considering this, Oxygen evolution may have occurred, as this event is common with materials with protective oxide films [47]. Additionally, Fig. 9 shows Alloy 3 and Alloy 4 at considerably different measured current densities during the test. These alloys are identical in the compositions, which may suggest the secondary phases, as well as crystallite sizes of the materials, may have an effect on their corrosion resistance. This effect is illustrated in Fig. 10, which shows potentiodynamic polarization curves of SPS processed alloys at different mechanical attrition times. Anodic corrosion current densities of alloy 1 increase with increasing mechanical attrition time. XRD analysis revealed the existence of a new phase that could be HCP α-phase or intermetallic phases. These secondary phases may be formed at longer milling times and could be the origin of the increased current density. Nonetheless, alloy 1 appears to readily repassivate at potentials higher than 2100 mV_{SCE} and the decreased current densities during the backward scan indicate that the alloy is protected. This supports the hypothesis modifying the microstructure by mechanical attrition may be favorable to corrosion resistance and could lead to alloys with advantageous corrosion rate and biocompatibility.

5. Conclusions

Ultrafine grained low modulus TNZT alloys were fabricated via mechanical alloying followed by spark plasma sintering using Bond order $\overline{B}_O$ and energy level $\overline{M}_D$ approach. All TNZT alloys have been sintered at 1373 K exhibited full densification.

- The microstructures of as fabricated TNZT alloys are composed of large volume fraction of BCC β-phase along with some minor fraction of HCP α-phase. XRD analysis confirmed a large volume fraction of the BCC β-phase structure attributed from the use of strong β-phase stabilizing elements Nb, Ta, and Zr.
- The microhardness of TNZT alloys fabricated via ball milling followed by spark plasma sintering using elemental blend powders is far higher than that of TNZT alloys fabricated by conventional powder metallurgy, casting, or sintered from pre-alloyed powders primarily due to refined grain structure obtained during ball milling as well as during spark plasma sintering process.
- The process of mechanical alloying of pure elemental powder, followed by SPS synthesis is an effective and novel procedure for processing low modulus β-phase titanium alloys for potential biomedical applications.
- The influence of the composition and processing in the corrosion behavior of TNZT alloys was investigated. All alloys exhibited high corrosion resistance. Considering excellent corrosion properties, these alloys are promising for future investigations on improving properties and studying underlying mechanisms.

CRediT authorship contribution statement

NM and TB: Conceptualization, Formal Analysis, Investigation, Methodology, Resources, Original draft; writing, review, and editing; TL: Investigation, Methodology; JE and RG: Investigation, Methodology, writing, review, and editing; RC: Investigation, Methodology.

Acknowledgements

This work is partially supported by the National Science Foundation under Grant No. 1126126.

References

[1] H.M. Kremers, D.R. Larson, C.S. Crowson, W.K. Kremers, R.E. Washington, C.A. Steiner, D.J. Berry, Prevalence of total hip and knee replacement in the United States, J. Bone Joint Surg. Am. 97 (17) (2015) 1386.
[2] S. Kurtz, K. Ong, E. Lau, F. Mowat, M. Halpern, Projections of primary and revision hip and knee arthroplasty in the United States from 2005 to 2030, JBJS 89 (4) (2007) 780–785.
[3] M. Niinomi, M. Nakai, Titanium-based biomaterials for preventing stress shielding between implant devices and bone, International Journal of Biomaterials 2011 (2011).
[4] N. Sumitomo, K. Noritake, T. Hattori, K. Morikawa, S. Niwa, K. Sato, M. Niinomi, Experiment study on fracture fixation with low rigidity titanium alloy, J. Mater. Sci. Mater. Med. 19 (4) (2008) 1581–1586.
[5] I. Gibson, D.W. Rosen, B. Stucker, Additive Manufacturing Technologies vol. 17, Springer, New York, 2014.
[6] M. Long, H.J. Rack, Titanium alloys in total joint replacement—a materials science perspective, Biomaterials 19 (18) (1998) 1621–1639.
[7] J.R. Davis, Concise Metals Engineering Data Book, ASM International, 1997.
[8] D. Kuroda, M. Niinomi, M. Morinaga, Y. Kato, T. Yashiro, Design and mechanical properties of new β type titanium alloys for implant materials, Mater. Sci. Eng. A 243 (1–2) (1998) 244–249.
[9] L.M. Zou, C. Yang, Y. Long, Z.Y. Xiao, Y.Y. Li, Fabrication of biomedical Ti–35Nb–7Zr–5Ta alloys by mechanical alloying and spark plasma sintering, Powder Metall. 55 (1) (2012) 65–70.
[10] E.W. Collings, The Physical Metallurgy of Titanium Alloys (Metals Park Ohio), 1984, p. 3.
[11] S. Nag, R. Banerjee, H.L. Fraser, Microstructural evolution and strengthening mechanisms in Ti–Nb–Zr–Ta, Ti–Mo–Zr–Fe and Ti–15Mo biocompatible alloys, Mater. Sci. Eng. C 25 (3) (2005) 357–362.
[12] M. Niinomi, Recent research and development in titanium alloys for biomedical applications and healthcare goods, Sci. Technol. Adv. Mater. 4 (5) (2003) 445.
[13] I. Kiyoshi, U.S. Patent No. 3,241,956, U.S. Patent and Trademark Office, Washington, DC, 1966.
[14] G. Weintraub, H. Rush, U.S. Patent No. 1,071,488, U.S. Patent and Trademark Office, Washington, DC, 1913.
[15] J.Y. Yang, J.S. Wu, T.J. Zhang, K. Cui, Multicomponent mechanical alloying of Fe–Cu–Nb–Si–B, J. Alloys Compd. 265 (1–2) (1998) 269–272.
[16] S. Azzaza, S. Alleg, J.J. Suñol, Phase transformation in the ball milled $Fe_{31}Co_{31}Nb_8B_{30}$ powders, Advances in Materials Physics and Chemistry 3 (01) (2013) 90.
[17] S. Alleg, S. Kartout, M. Ibrir, S. Azzaza, N.E. Fenineche, J.J. Suñol, Magnetic, structural and thermal properties of the Finemet-type powders prepared by mechanical alloying, J. Phys. Chem. Solids 74 (4) (2013) 550–557.
[18] S. Alleg, M. Ibrir, N.E. Fenineche, S. Azzaza, R. Bensalem, J.J. Suñol, Magnetic and structural characterization of the mechanically alloyed $Fe_{75}Si_{15}B_{10}$ powders, J. Alloys Compd. 494 (1–2) (2010) 109–115.
[19] B.S. Murty, S. Ranganathan, Novel materials synthesis by mechanical alloying/milling, Int. Mater. Rev. 43 (3) (1998) 101–141.
[20] C. Suryanarayana, Mechanical alloying and milling, Prog. Mater. Sci. 46 (1–2) (2001) 1–184.
[21] L. Schultz, Formation of amorphous metals by mechanical alloying, Mater. Sci. Eng. 97 (1988) 15–23.
[22] Y.J. Liu, I.T.H. Chang, P. Bowen, Amorphization and microstructural evolution in multicomponent (FeCoNi) 70Zr10B20 alloy system by mechanical alloying, Mater. Sci. Eng. A 304 (2001) 389–393.
[23] A.W. Weeber, H. Bakker, Amorphization by ball milling. A review, Phys. B Condens. Matter 153 (1–3) (1988) 93–135.
[24] C.C. Koch, Amorphization by mechanical alloying, J. Non-Cryst. Solids 117 (1990) 670–678.
[25] S. Surinach, M.D. Baro, J. Segura, M.T. Clavaguera-Mora, N. Clavaguera, Amorphization of soft magnetic alloys by the mechanical alloying technique, Mater. Sci. Eng. A 134 (1991) 1368–1371.
[26] M.H. Enayati, F.A. Mohamed, Application of mechanical alloying/milling for synthesis of nanocrystalline and amorphous materials, Int. Mater. Rev. 59 (7) (2014) 394–416.
[27] D.L. Zhang, Processing of advanced materials using high-energy mechanical milling, Prog. Mater. Sci. 49 (3–4) (2004) 537–560.
[28] Z.A. Munir, D.V. Quach, M. Ohyanagi, Electric current activation of sintering: a review of the pulsed electric current sintering process, J. Am. Ceram. Soc. 94 (1) (2011) 1–19.
[29] Q. Li, G. Wang, X. Song, L. Fan, W. Hu, F. Xiao, Q. Yang, M. Ma, J. Zhang, R. Liu, Ti50Cu23Ni20Sn7 bulk metallic glasses prepared by mechanical alloying and spark-plasma sintering, J. Mater. Process. Technol. 209 (7) (2009) 3285–3288.
[30] S.P. Harimkar, T. Borkar, A. Singh, Spark plasma sintering of amorphous-crystalline laminated composites, Mater. Sci. Eng. A 528 (3) (2011) 1901–1905.
[31] X.H. Wang, W.A.N.G. Ge, Y.Y. Zhu, J.F. Bao, X.F. Du, L.I. Qiang, Fe75Zr3Si13B9 magnetic materials prepared by spark plasma sintering, Trans. Nonferrous Metals Soc. China 24 (3) (2014) 712–717.
[32] S. Lee, H. Kato, T. Kubota, A. Makino, A. Inoue, Fabrication and soft-magnetic properties of Fe–B–Nb–Y glassy powder compacts by spark plasma sintering technique, Intermetallics 17 (4) (2009) 218–221.
[33] X. Li, A. Makino, H. Kato, A. Inoue, T. Kubota, Fe76Si9. 6B8. 4P6 glassy powder soft-magnetic cores with low core loss prepared by spark-plasma sintering, Mater. Sci. Eng. B 176 (15) (2011) 1247–1250.
[34] B. Shen, A. Inoue, H. Kimura, M. Omori, A. Okubo, Bulk glassy soft-magnetic cores produced by spark-plasma sintering Fe65Co10Ga5P12C4B4 glassy powder, Mater. Sci. Eng. A 375 (2004) 666–670.
[35] K. Vinathi Reddy, Osseointegration, International Dental & Medical Journal of Advanced Research 1 (2015) 1–7.
[36] P.F. Santos, M. Niinomi, K. Cho, M. Nakai, H. Liu, N. Ohtsu, T. Narushima, Microstructures, mechanical properties and cytotoxicity of low cost beta Ti–Mn alloys for biomedical applications, Acta Biomater. 26 (2015) 366–376.
[37] M. Morinaga, M. Kato, T. Kamimura, M. Fukumoto, I. Harada, K. Kubo, Theoretical design of beta-type titanium alloys, in: Titanium'92: Science and Technology, 1993, pp. 217–224.
[38] M. Abdel-Hady, K. Hinoshita, M. Morinaga, General approach to phase stability and elastic properties of β-type Ti-alloys using electronic parameters, Scr. Mater. 55 (5) (2006) 477–480.
[39] J. Geiser, Coupled Systems: Theory, Models, and Applications in Engineering, Chapman and Hall/CRC, 2014.
[40] R. Banerjee, S. Nag, J. Stechschulte, H.L. Fraser, Strengthening mechanisms in Ti–Nb–Zr–Ta and Ti–Mo–Zr–Fe orthopaedic alloys, Biomaterials 25 (17) (2004) 3413–3419.
[41] A.H. Hussein, M.A.H. Gepreel, M.K. Gouda, A.M. Hefnawy, S.H. Kandil, Biocompatibility of new Ti–Nb–Ta base alloys, Mater. Sci. Eng. C 61 (2016) 574–578.
[42] R.Z. Valiev, V.V. Stolyarov, H.J. Rack, T.C. Lowe, SPD-processed ultra-fine grained ti materials for medical applications, Medical Device Materials (2004) 362–367.
[43] G. Lütjering, J.C. Williams, Titanium, Springer Science & Business Media, 2007.
[44] S.A. Souza, R.B. Manicardi, P.L. Ferrandini, C.R.M. Afonso, A.J. Ramirez, R. Caram, Effect of the addition of Ta on microstructure and properties of Ti–Nb alloys, J. Alloys Compd. 504 (2) (2010) 330–340.
[45] F. Zhang, M. Reich, O. Kessler, E. Burkel, The potential of rapid cooling spark plasma sintering for metallic materials, Mater. Today 16 (5) (2013) 192–197.
[46] P. Mausli, Properties of surface oxides on titanium and some titanium alloys, in: Sixth World Conference on Titanium. IV, 1988, June, pp. 1759–1764.
[47] D.G. Enos, L.L. Scribner, The potentiodynamic polarization scan, Solartron Instruments, Hampshire, UK, Technical Report 33 (1997).